Available online at www.eccomasproceedia.org
Eccomas Proceedia COMPDYN (2021) 3912-3929

ECCOMAS
Proceedia

COMPDYN 2021
8th ECCOMAS Thematic Conference on
Computational Methods in Structural Dynamics and Earthquake Engineering
M. Papadrakakis, M. Fragiadakis (eds.)
Streamed from Athens, Greece, 28 - 30 June 2021

SEISMIC PERFORMANCE OF STRUCTURES EQUIPPED WITH BRB

P. Castaldo[1], E. Tubaldi[2], and L. Gioiella[3]

[1] Department of Structural, Geotechnical and Building Engineering (DISEG),
Politecnico di Torino, Turin, Italy
paolo.castaldo@polito.it
[2] Department of Civil and Environmental Engineering,
University of Strathclyde, Glasgow, Scotland
enrico.tubaldi@strath.ac.uk
[3] School of Architecture and Design SAAD,
University of Camerino, Ascoli Piceno, Italy,
laura.gioiella@unicam.it

Abstract

Over the years, the buckling restrained braces (BRBs) have more and more become one of the best solutions for retrofitting or upgrading many existing reinforced concrete framed buildings located in areas with a high seismic hazard. The present investigation studies the effectiveness of BRBs used to seismically retrofit a reinforced concrete (RC) building in L'Aquila defining an advanced non-linear 3D model in OpenSees. The seismic performance of the investigated building is assessed developing the following comparisons: before and after the retrofit through BRBs. Adopting a hysteretic model specific for the BRBs, both non-linear static analyses and incremental dynamic analyses under a set of real ground motion records are carried out to build the seismic demand hazard curves. The numerical results highlighted the influence of the BRBs on the seismic performance of the system components also in relation to the effectiveness of the retrofit.

Keywords: Seismic Demand Hazard Curves, Buckling Restrained Braces, Capacity, Reinforced Concrete Frame, Masonry Infill Walls.

ISSN:2623-3347
Peer-review under responsibility of the organizing committee of COMPDYN 2021.
doi: 10.7712/120121.8756.18551

1 INTRODUCTION

Among the different solutions available to enhance the performance of existing structures, a great variety of passive energy dissipation systems [1]-[3] have been proposed in the last decades. These systems are usually classified as hysteretic dampers, viscoelastic dampers, viscous fluid dampers [4] and friction dampers [5]. Buckling restrained braces (BRBs) are hysteretic dampers that constitute one of the most efficient system for adding stiffness, strength and energy dissipation capacity to a structure [6]-[8]. The effectiveness of these devices has been proven by many experimental tests and numerical simulations, and numerous applications to existing buildings have been documented in the literature (e.g., [9]-[12]). BRBs consist of a steel core placed inside a steel tube filled with a concrete material [13]-[14]. According to numerous experimental tests, BRBs exhibit a stable hysteretic behaviour with a high-energy dissipation capacity, up to ductility levels higher than 20 [15]-[16].

Many studies in the literature have proposed methodologies for the design of BRBs for retrofitting existing frames and have evaluated the performance of the retrofit with deterministic approaches (e.g., [17]-[19]). However, very few works have analyzed the performance of buildings retrofitted with BRBs by employing probabilistic approaches accounting for the effect of the uncertainties inherent to the seismic input. Among these, Guneysi [20] investigated the application of BRBs for seismic retrofitting of steel moment resisting framed buildings. Fragility curves were developed using the maximum interstorey drift ratio as engineering demand parameter (EDP), and were used to compare the performances of the bare frame, the frame retrofitted with conventional braces, and the frame retrofitted with BRBs. Freddi et al. [7] proposed a probabilistic framework, based on the use of component and system fragility curves, to evaluate the effectiveness of BRBs for retrofitting reinforced concrete (RC) frames with low ductility capacity. Moreover, important EDPs, such as the absolute accelerations, were disregarded. Adding stiffness and strength to a frame through the BRBs often leads to an increase rather than a decrease of absolute accelerations, due to the reduction of the vibration period, and this may affect the performance of acceleration-sensitive non-structural building components. Furthermore, it is widely acknowledged that the main drawback of BRBs is their low post-yield stiffness, which may result in excessive residual inter-storey drifts in structures equipped with them [21]-[23]. Thus, an assessment of the effectiveness of the retrofit should also account for the response in terms of these two EDPs.

Finally, previous studies on the performance of buildings retrofitted with BRBs have employed simplified models of the BRBs with essentially elasto-plastic behaviour and kinematic hardening. However, more sophisticated constitutive models should be considered to properly account for the specific features of the behaviour of these devices that emerged in numerous experimental tests [13], [24]-[25]. These include the significant role of isotropic hardening and the asymmetry in the yield force in compression with respect to that in tension [13], [24]. The cumulative plastic deformations in the BRBs, that may control the failure of these devices due to low-cycle fatigue, need also to be monitored [26]-[31].

The aim of this work is to evaluate the effectiveness of buckling restrained braces for retrofitting an existing RC building, by employing an advanced model of BRBs and a wide range of EDPs for monitoring the performance of the building components and of the BRBs. For this purpose, an existing RC building located in L'Aquila, damaged by the 2009 earthquake, is used as case study. First, a non-linear three-dimensional model of the existing RC building is defined in OpenSees [32]. A widely employed procedure based on pushover analyses and N2 method [33] is employed to design the braces. Specifically, the bracing system is designed by disregarding the effect of infill walls and with the target objective of achieving a maximum interstorey drift ratio of 1.5% under the life safety limit state design seismic action [34] for the

site (return period of 475 years). Successively, the seismic performance of the retrofitted building is evaluated by performing both non-linear static analyses and incremental dynamic analyses under a set of real ground motion records. Seismic fragility and demand hazard curves of the building are derived considering multiple EDPs. These include the maximum interstorey drifts together with the absolute accelerations.

The capability of the dissipative bracing system in enhancing the performance of structural and non-structural components of the frame is assessed by evaluating the results in terms of seismic demand hazard curves, providing the annual rate exceeding different demand levels.

2 CASE STUDY: DESCRIPTION AND MODELLING

The case study (Figure 1) is a reinforced concrete frame built in 1984 that is representative of many RC structures built in Italy before the introduction of modern seismic codes and designed for gravity loads only, without any seismic detailing. The building is composed of five stories with a height of 2.8 m at the ground storey and of 3 m at the other storeys. Figure 1 describes the plan configuration of the frame, with an overall length of 25.30x10.85 m along the horizontal (X) and vertical (Y) directions, respectively. A reinforced concrete staircase is located centrally in the lower part of the building. The frame columns have a rectangular cross section with dimensions 35x60 cm at the ground floor and 30x60 cm at the other floors, whereas the columns that support the stair landing have the same rectangular cross section of 25x60 cm at each floor. The beams along the Y direction are deep beams with various rectangular sections: 35x50 cm, 30x50 cm and 25x50 cm. The properties of materials used for the structural components of the frame have been evaluated via a campaign of destructive in-situ tests. In particular, the concrete material behavior was evaluated based on 16 compressive tests on concrete cores extracted from the RC frame elements, while the steel properties were evaluated based on tensile strength tests executed on rebar samples. Table 1 reports the average mechanical properties for unconfined concrete and reinforcement steel. With regards to concrete, f_c denotes the compressive strength, E_c the elastic modulus, ε_c and ε_{cu} the peak and ultimate deformations, and f_{cu} the ultimate strength. With regards to steel, f_{sy} is the yield stress, E_s the elastic modulus, and *b* the post-elastic to elastic stiffness hardening ratio.

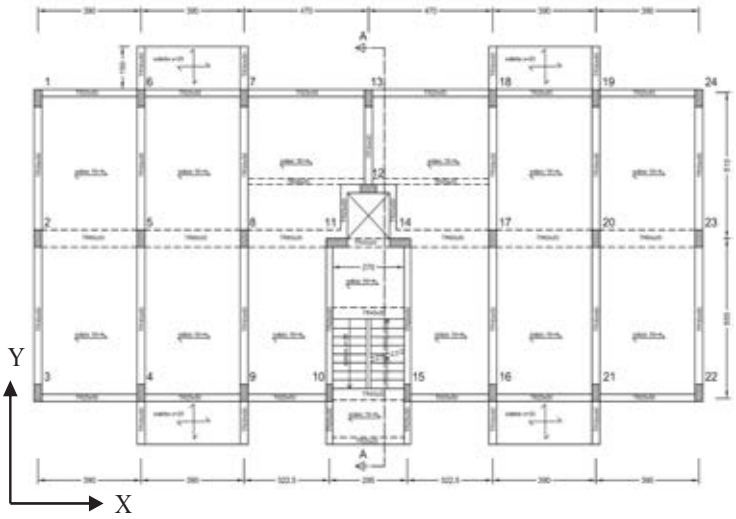

Figure 1. Schematic plan configuration of the building. (Dimensions in cm)

Unconfined concrete					Steel		
f_{cm} [N/mm^2]	ε_c [-]	f_{cu} [N/mm^2]	ε_{cu} [N/mm^2]	E_c [N/mm^2]	f_{sy} [N/mm^2]	E_s [N/mm^2]	b [-]
21.6	0.018	21.6	0.0035	27717.8	430.7	206000	0.01

Table 1. Mechanical properties of unconfined concrete and steel reinforcement.

The building is located in L'Aquila (Italy), with geographical coordinates Lon. = 13.394° and Lat. = 42.36°, on a soil of class D and topographical category T1, according to [34]. Figure 2 shows the code elastic response spectra in terms of accelerations and displacements for different limit states and relevant return periods (i.e., Operational – 30 years, Damage – 50 years, Life Safety – 475 years, Near Collapse - 975 years) assuming an inherent damping factor of 5%, respectively.

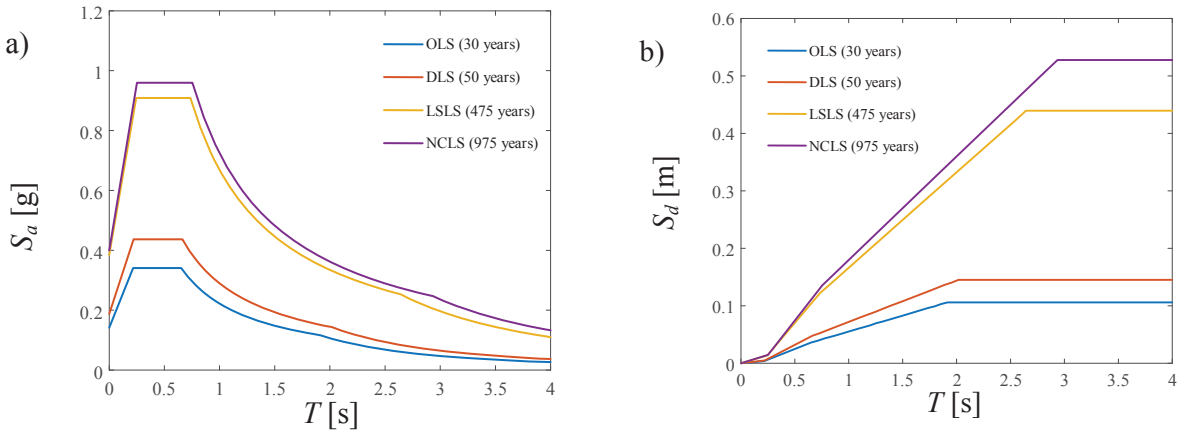

Figure 2. Code elastic response spectra in terms of accelerations a) and displacements b).

Figure 3 shows the numerical model of the RC frame developed in OpenSees [32], which employs "beam with hinges" elements [35] to describe the nonlinear hysteretic response of beams and columns. The beam-column joints are described by beam elements with very high stiffness whereas the in-plane rigid floor slab is described by a diaphragm constraint at each floor. In the "beam with hinges" elements, the inelastic behaviour is concentrated over specified hinge lengths L_{pi} and L_{pj} at the two element ends while, a linear elastic behaviour is assigned to the central portion. The lengths of the plastic hinges are defined as a function of the shear span L_V, assumed equal to the half element length, and of the product between the bar yield strength and diameter $f_{sy}d_b$ [36]:

$$L_p = 0.12L_V + 0.014\alpha_{sl}f_{sy}d_b \tag{1}$$

where α_{sl} is a variable that can assume the value 1 if the slippage of the reinforcement bars from the anchorage zone beyond the end section is possible or 0 if is not.

In the plastic hinge zone, the behaviour of concrete is described by the nonlinear degrading Concrete02 material model [32], with tensile strength set to $0.1f_{cm}$ and a linear tension softening.

The effect of the confinement of the concrete core fibers of beams and columns is taken into account by modifying the concrete constitutive law as suggested by [37]. The compressive

strength of the confined concrete increases thanks to the compressive effect provided by the stirrups and the longitudinal reinforcement and can be evaluated as:

$$f_{cc}^{'} = f_{cm}\left(-1.254 + 2.254\sqrt{1+\frac{7.94 f_l^{'}}{f_{cm}}} - 2\frac{f_l^{'}}{f_{cm}}\right) \tag{2}$$

where f_{cm} is the compressive strength of the unconfined concrete (Table 1) and $f_l^{'}$ depends on the geometry of the section and of the reinforcements as explained in [37]. The ultimate compressive strain, ε_{cu}, corresponds to the rupture of the first hoop and can be found based on an energy balance approach [37]. The confinement differs for each section, since it depends on the dimensions, and amount of longitudinal bars and stirrups. Thus, different values of $f_{cc}^{'}$, crushing strength and ε_{cu} are obtained for the various sections.

The behaviour of steel reinforcement is described by using a uniaxial bilinear constitutive law with kinematic hardening (Steel01 in OpenSees [32]). Concrete cracking is taken into account by considering an effective flexural stiffness for the elastic part of each beam and column element. This stiffness is evaluated by means of moment-curvature analysis of the sections at the extremes of the elements, for the axial force level induced by the dead loads (zero axial load in case of beams).

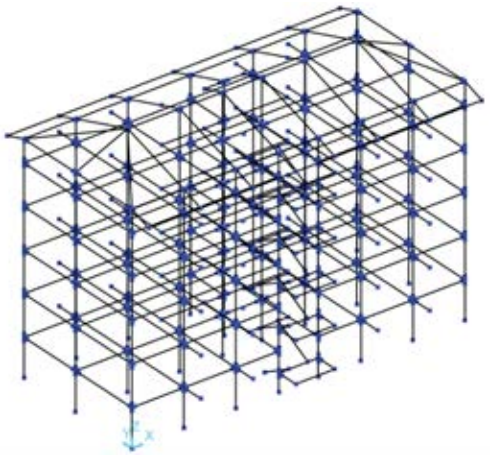

Figure 3. Numerical model of the RC building in OpenSees (with no infills).

Using the function "MinMax material" of OpenSees [32], material failure can be simulated in the fibers of the RC sections by setting the stresses to zero once a prefixed strain threshold value is attained. Conservatively, the same threshold of ε_{cu} equal to -0.012 is set for all the concrete fibers with the confined properties. For the unconfined concrete of the cover of the cross sections, the strain threshold was set to -0.0035. The rupture of the reinforcement bars, with a drop of the stress to zero, is assumed to occur at a strain of 0.075. The system nonlinear geometrical behaviour is taken into account by considering second-order P-delta effects.

3 DESIGN AND MODELLING OF THE HYSTERETIC DEVICES (BRBS)

The method proposed by Dall'Asta et al. [17] is employed in this study to design the dissipative bracing system. According to this method, the dissipative bracing system and the existing frame are described as two elastic-perfectly plastic single-degree-of-freedom (SDOF) systems acting in parallel. The properties of the SDOF system equivalent to the existing frame

are derived by performing a pushover analysis under a distribution of forces corresponding to its first vibration mode [33]. The capacity curve of the frame is replaced by an elastic perfectly-plastic one, which is obtained based on an energy equivalence criterion and is described by the initial stiffness K_f, the base shear capacity V_f, and the ductility capacity μ_{fc} (Figure 4a).

The properties of the bracing system depend on the properties of the diagonal braces at each storey. It is worth to recall that the diagonal dissipative braces considered here consist of two members in series, namely the BRB device and the over-strengthened brace. Only the first one undergoes plastic deformations, whereas the second is designed to remain elastic.

The distribution of the stiffness of the braces along the building height is assumed equal to the one of the frame in order to obtain a coupled system with the same first mode shape. Moreover, the braces are assumed to yield simultaneously when the structure vibrates according to the first mode.

The design ultimate displacement of the diagonal brace system can be assumed equal to that of the frame, in order to ensure simultaneous failure of both the frame and the braces. The capacity curve of the bracing system is idealized as an elastic-perfectly plastic curve, and described by few parameters that are the design variables: the initial stiffness K_d, the base shear capacity V_d, and ductility capacity μ_{dc}, equal to that of the diagonal braces under the assumption of simultaneous yielding of the diagonal braces at all the storeys. It is noteworthy that the BRBs, and thus the bracing system, exhibit a more complicated behaviour, which however is simplified in the design stage.

In this study, only the retrofit of the frame along the X direction is considered, since this corresponds to the weak direction of the bare frame. The results from the modal analysis of the bare frame for the first five vibration modes are summarized in Table 2. The coupling between the modal responses along the two directions is very low, and the mass participation factor of the first mode along the X direction is very high (i.e., 80.8%).

Mode	Type	ω [rad/s]	T [s]
1	Translational X	7.388	0.850
2	Rotational	9.371	0.670
3	Translational Y	9.496	0.662
4	Translational X	23.432	0.268
5	Rotational	30.300	0.207

Table 2. Vibration modes of the bare frame.

The design procedure of the bracing system requires the evaluation of the bare frame capacity curve along the X direction by means of a nonlinear static (pushover) analysis. The lateral load pattern for the pushover analysis is determined for a distribution of the loads proportional to the first vibration mode of the structure. The control node is the centre of mass of the top floor. Figure 4a shows the capacity curve of the equivalent SDOF system and its bilinearization according to the Italian code [34]. These curves are expressed in terms of d^* and V^*, which are obtained dividing the displacement of the control node and the base shear of the MDOF system by the modal participation factor $\Gamma = \sum m_i u_i \big/ \sum m_i u_i^2$ of the first vibration mode. The ductility capacity of the frame is μ_{fc} =3.73, corresponding to a maximum interstorey drift ratio of 2.3%.

Figure 4b compares, in the acceleration-displacement plane, the elasto-plastic capacity curve of the bare frame and the seismic demand for the life safety limit state according to the N2 method. The values of the acceleration a^* of the capacity curve are obtained by dividing the forces V^* by the equivalent mass $m^* = \sum m_i \mu_i$ of the SDOF system. It can be seen that the ductility demand μ_f=3.55 is quite close to the ductility capacity of the structure. Thus, the structure needs to undergo significant plastic deformations to withstand the seismic demand, leading to extended damage.

In order to reduce the seismic damage, the bracing system is added in parallel to the frame, and the target ductility demand of the frame under the design seismic input is assumed equal to μ_f=2.64, corresponding to a maximum interstorey drift ratio (IDR) of 1.5%.

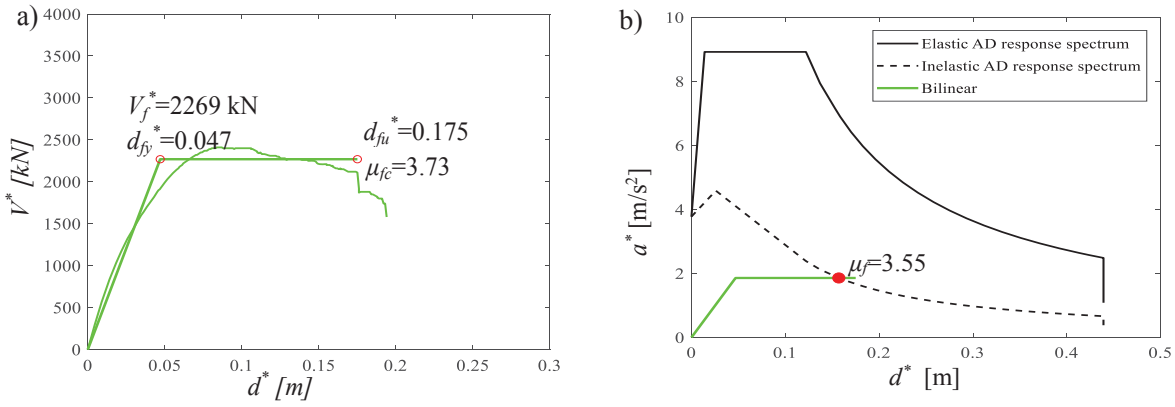

Figure 4. a) Capacity curve of the SDOF system equivalent to the bare frame and its bi-linearization and b) comparison between the seismic demand and capacity for the bare frame.

The ductility capacity of the BRB devices and of the dissipative system are assumed respectively equal to μ_{0c}=15 and μ_{dc}=10. It is noteworthy that the value of μ_{dc} is less than the value of μ_{0c} due to the flexibility of the brace placed in series with the BRB device ([6], [17]). The base shear capacity of the BRB system must be equal to V_d=900 kN to obtain a design capacity curve of the coupled system (frame and BRBs system) that intersects the inelastic demand spectrum (Figure 5a-b). It is noteworthy that the base shear of the bracing system is only 39% of the base shear of the bare frame. Although a higher value could be chosen, by reducing the ductility demand of the frame, this would result in excessive forces transmitted to the columns adjacent to the bracing system, and an increase of their vulnerability [6]. Moreover, higher values of this ratio are generally associated with excessive interstorey residual drift levels, impairing reparability after major earthquake events.

Given the properties of the bracing system, the characteristics of the BRB devices and of the elastic braces at each storey can be determined by following the procedure described in Dall'Asta et al. [17] and they are reported in Table 3. It is worth to recall that the design properties of the braces (initial stiffness K_d^i, yielding force F_d^i and ductility capacity μ_{dc}^i where i denotes the storey number) depend on the properties of the BRB device (initial stiffness K_0^i, yield force F_0^i and ductility capacity μ_{0c}^i) and on the properties of the elastic brace (length L_b^i and stiffness K_b^i). The brace length L_d^i is equal to the sum of the BRB length L_0^i and the elastic brace length L_b^i.

In order to limit the axial forces transmitted to the columns adjacent to the braces, four diagonal braces are employed at each storey. The brace arrangement is shown in Figure 6.

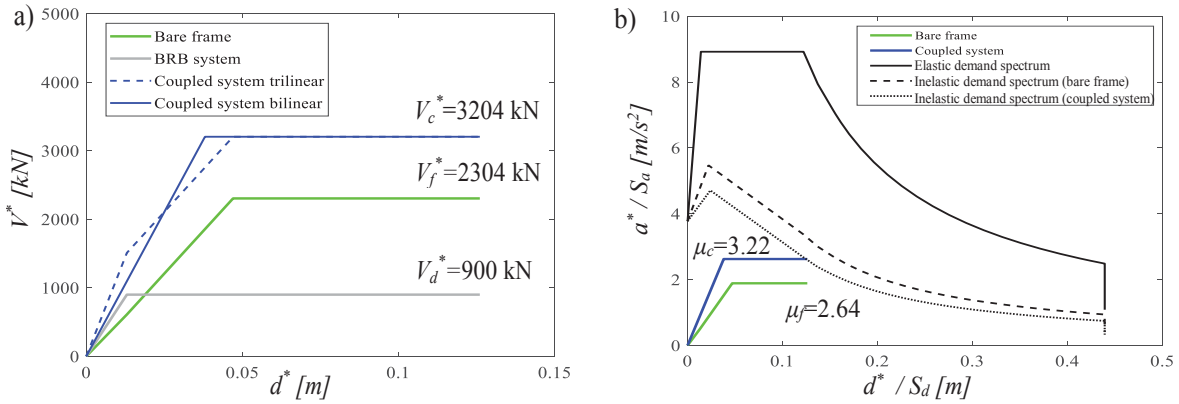

Figure 5. a) Design bilinear capacity curve of the SDOF system equivalent to the retrofitted frame and b) comparison between the seismic demand and capacity for the retrofitted frame.

	Braces		BRBs				Elastic braces				
Storey	F_c^i	K_c^i	K_0^i	F_0^i	A_0^i	L_0^i	K_b^i	F_b^i	A_b^i	t_b^i	L_b^i
[-]	**[kN]**	**[kN/m]**	**[kN]**	**[kN/m]**	**[m^2]**	**[m]**	**[kN]**	**[kN/m]**	**[m^2]**	**[mm]**	**[m]**
4	152	91404	142.18	152.05	608.19	898.3	142.18	152.05	608.19	10	898.3
3	235.6	91793	142.79	235.56	942.23	1385.7	142.79	235.56	942.23	10	1385.7
2	299	95200	148.09	299.04	1196.14	1696.2	148.09	299.04	1196.14	10	1696.2
1	338	105238	163.7	337.99	1351.97	1734.3	163.7	337.99	1351.97	10	1734.3
0	343.8	188593	293.37	343.78	1375.14	984.4	293.37	343.78	1375.14	10	984.4

Table 3. Dissipative braces, BRBs and elastic brace properties at each storey.

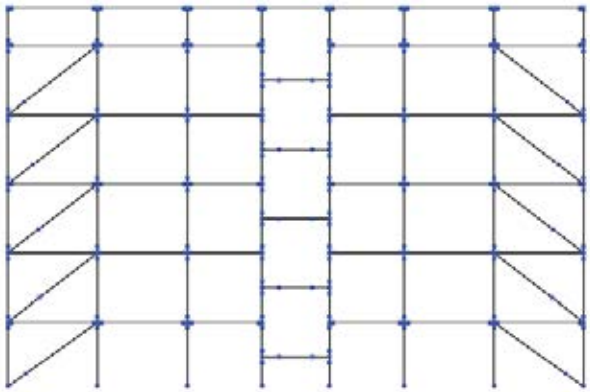

Figure 6. Modelling of the BRB by means of two elements (truss + elastic beam).

The dissipative braces are modelled by using two elements (Figure 6): an elastic beam element for the elastic brace and a truss element for the BRB. The BRB is assigned the constitutive law of Zona et al. [30]. The parameters that influence the hardening and hysteresis of the elasto-plastic model can be calibrated based on experimental characterization tests carried out on BRB prototypes. In this study, the parameters reported in Zona et al. [30] and calibrated on

the experimental tests of Tremblay et al. [38] are considered. Figure 7 shows the capacity curve evaluated by performing the nonlinear static analysis of the retrofitted structure, and the corresponding equivalent bilinear curve. The capacity curve is truncated at a value of the displacement equal to 0.15 m, corresponding to an IDR of 1.5% for the frame and a ductility capacity μ_c=3.22. The ductility of the coupled system is much higher than that of the frame (μ_f=2.64), thanks to the addition of the BRBs. Figure 7b compares the elastic and inelastic seismic demand with the capacity of the coupled system. The seismic design action induces a ductility demand of 3.13 (Figure 7b) in the system.

It is noteworthy that the design of the dissipative bracing system has been carried out disregarding the contribution of the infill walls.

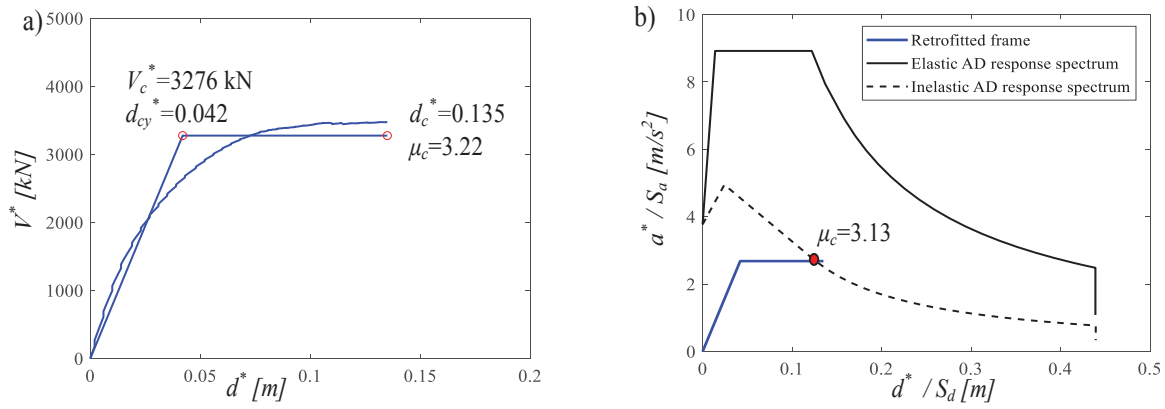

Figure 7. a) Capacity curve of the SDOF system equivalent to the retrofitted system and its bi-linearization and b) comparison between the seismic demand and capacity for the retrofitted frame.

4 SEISMIC PERFORMANCE AND RETROFIT EFFECTIVENESS EVALUATION

The seismic performance assessment of the system and the evaluation of the effectiveness of BRBs for the retrofit are based on the development and comparison of seismic demand hazard curves for different EDPs describing the seismic response of structural and non-structural components, as well as of the BRBs. Coherently with the performance-based earthquake engineering (PBEE) approach [39]-[41], the uncertainties related to the seismic input intensity are separated from those related to the characteristics of the record (i.e., record-to-record variability) by introducing an intensity measure (*IM*). In particular, the randomness in the seismic intensity is described by a hazard curve, whereas the record-to-record variability for a fixed intensity level is modelled by selecting a set of natural ground motion records characterized by a different duration and frequency content, scaled to the assumed intensity level [42].

It is worth to note that, in general, the *IM*'s choice should be driven by criteria of efficiency, sufficiency and hazard computability [43]-[45]. In this study, the spectral acceleration, $S_a(\xi, T)$, at the fundamental period of the system, $T = 2\pi / \omega$ and for the damping ratio ξ =5%, is assumed as intensity measure. This is a structural dependent *IM* that changes with the structural model. Table 4 reports the periods of the four models considered, together with the corresponding *IM* values at the life safety limit state (LFLS) and near collapse limit state (CLS).

Incremental dynamic analysis (IDA) [46] are carried out to investigate the response of the different systems for increasing intensity levels. The set of 30 ground motion records employed in IDA are derived from 19 different seismic natural events, selected within the ground motion database of PEER (Pacific Earthquake Engineering Research Center) [47], of ITACA

(Italian Accelerometric Archive) [48] and of ISESD (Internet-Site for European Strong-Motion Data) [49]. The characteristics of the selected ground motion records are reported in Table 5. Their source-to-site distance, R_s, is greater than 8.7 km, and their moment magnitude, M, is in the range between 6 and 7.6. Figure 8 shows the acceleration elastic response spectra of the unscaled records of Table 5.

	Bare frame	**Retrofitted frame**	**Infilled frame**	**Inf. retrofitted frame**
T **[s]**	0.850	0.637	0.836	0.632
$S_{a,LSLS}$ **[g]**	0.787	0.909	0.799	0.909
$S_{a,NCLS}$ **[g]**	0.851	0.959	0.865	0.959

Table 4. Periods of the four models.

#	Year	Earthquake Name	Recording Station Name	Vs_{30} [m/s]	Fault Type	M [-]	R_s[km]	PGA [g]
1	1994	Northridge	Beverly Hills - Mulhol	356	Thrust	6.7	13.3	0.52
2	1994	Northridge	Canyon Country-WLC	309	Thrust	6.7	26.5	0.48
3	1994	Northridge	LA-Hollywood Stor	316	Thrust	6.7	22.9	0.36
4	1999	Duzce, Turkey	Bolu	326	Strike-slip	7.1	41.3	0.82
5	1999	Hector Mine	Hector	685	Strike-slip	7.1	26.5	0.34
6	1979	Imperial Valley	Delta	275	Strike-slip	6.5	33.7	0.35
7	1979	Imperial Valley	El Centro Array #11	196	Strike-slip	6.5	29.4	0.38
8	1995	Kobe, Japan	Nishi-Akashi	609	Strike-slip	6.9	8.7	0.51
9	1995	Kobe, Japan	Shin-Osaka	256	Strike-slip	6.9	46.0	0.24
10	1999	Kocaeli, Turkey	Duzce	276	Strike-slip	7.5	98.2	0.36
11	1999	Kocaeli, Turkey	Arcelik	523	Strike-slip	7.5	53.7	0.22
12	1992	Landers	Yermo Fire Station	354	Strike-slip	7.3	86.0	0.24
13	1992	Landers	Coolwater	271	Strike-slip	7.3	82.1	0.42
14	1989	Loma Prieta	Capitola	289	Strike-slip	6.9	9.8	0.53
15	1989	Loma Prieta	Gilroy Array #3	350	Strike-slip	6.9	31.4	0.56
16	1990	Manjil, Iran	Abbar	724	Strike-slip	7.4	40.4	0.51
17	1987	Superstition Hills	El Centro Imp. Co.	192	Strike-slip	6.5	35.8	0.36
18	1987	Superstition Hills	Poe Road (temp)	208	Strike-slip	6.5	11.2	0.45
19	1987	Superstition Hills	Westmorland Fire Stat.	194	Strike Slip	6.5	15.1	0.21
20	1992	Cape Mendocino	Rio Dell Overpass	312	Thrust	7.0	22.7	0.55
21	1999	Chi-Chi, Taiwan	CHY101	259	Thrust	7.6	32	0.44
22	1999	Chi-Chi, Taiwan	TCU045	705	Thrust	7.6	77.5	0.51
23	1971	San Fernando	LA - Hollywood Stor	316	Thrust	6.6	39.5	0.21
24	1976	Friuli, Italy	Tolmezzo	425	Thrust	6.5	20.2	0.35
25	1980	Irpinia	Bisaccia	496		6.9	21.3	0.94
26	1979	Montenegro	ST64	1083	Thrust	6.9	21.0	0.18
27	1997	Umbria Marche	ST238	n/a	Normal	6.0	21.5	0.19
28	2000	South Iceland	ST2487	n/a	Strike Slip	6.5	13	0.16
29	2000	South Iceland (a.s.)	ST2557	n/a	Strike Slip	6.4	15.0	0.13
30	2003	Bingol	ST539	806	Strike Slip	6.3	14.0	0.30

Table 5. Selected ground motions for the time history analyses.

The EDPs considered for monitoring the seismic response are the peak values, among the various storeys, of the interstorey drift ratio (IDR) and the absolute acceleration (ACC).

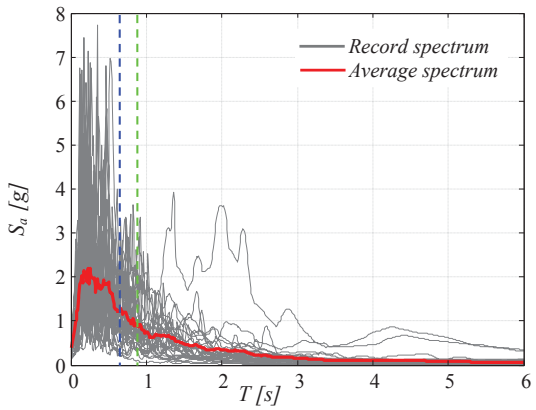

Figure 8. Acceleration elastic response spectra for the seismic records. The dashed lines indicate the structural periods of the various models.

Figure 9 shows the IDA curves in terms of IDR obtained for the various models considered. It is noteworthy that for high *IM* values, some convergence issues arise due to the failure of some fibers in critical sections and nonlinear geometrical behaviour of the model. Thus, plotted in the figure are only the numerically-converging dynamic analysis points. It can be observed in the plot that in the case of the bare frame, the IDR of 1.5% is reached at an *IM* = 0.3g for the bare frame model and at 0.7g for the retrofitted model. This results already shows the benefit of the use of the BRBs in terms of drift reduction, which is only partially impaired by the seismic demand increase due to period reduction (see Table 4).

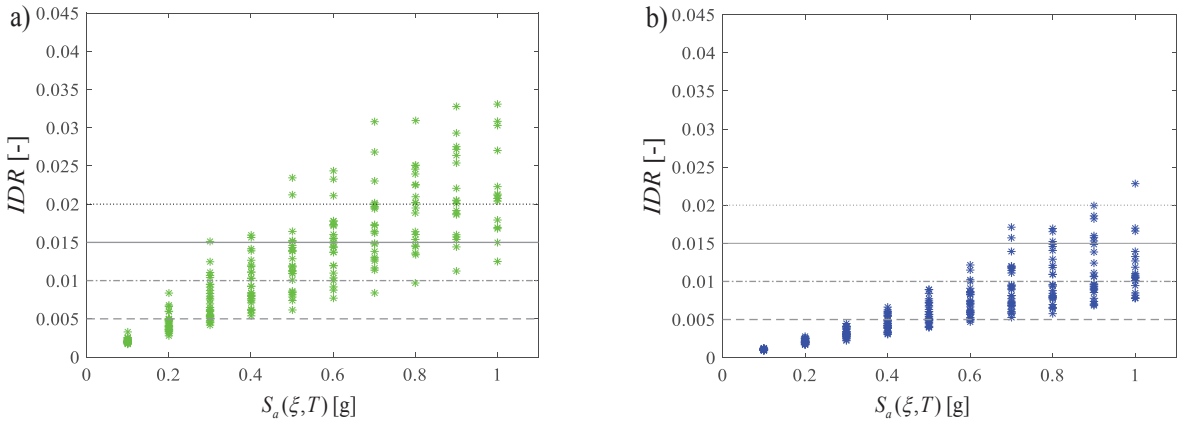

Figure 9. IDA results in terms of IDR: a) Bare frame; b) Bare frame with BRBs.

For each EDP considered, the conditional exceeding probability $G_{EDP|IM}(d|im)$ is evaluated for the different models at the various *IM* levels considered. Both the collapse (and convergence) and not-collapse results are taken into account by applying the total probability theorem [50]-[53], according to the following expression:

$$G_{EDP|IM}(edp|im) = G_{EDP|IM}(edp|im, NC)\left(1 - P\left[C|IM\right]\right) + P\left[C|IM\right] \tag{3}$$

where $G_{EDP|IM}(edp|im, NC)$ is the probability of exceedance of the EDP conditional to the *IM* and to not-collapse, the probability of collapse $P[C|IM]$ is evaluated numerically for each *IM* level by dividing the number of analyses for which collapse occur by the total number of analyses.

Figure 10 shows the conditional exceedance curves for the IDRs, which are fitted by means of lognormal distributions. Five different demand thresholds are considered, namely 0.5%, 1%, 1.5%, 2% and 2.5%. These values correspond to increasing levels of seismic damage of the frame [50], [51], [54]. Obviously, the median value of the spectral acceleration corresponding to the threshold of 1.5% increases due to the retrofit and slightly decreases if the infill frames are considered in the models.

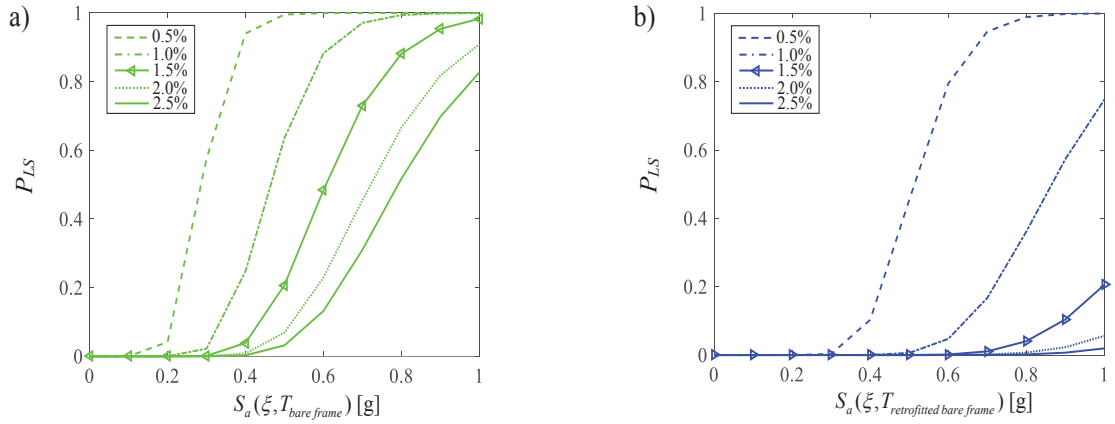

Figure 10. Conditional probability of exceedance vs. IM for the IDR: a) Bare frame; b) Bare frame with BRBs.

Figure 11 illustrates the conditional exceedance curves for the other EDP. In general, the exceeding probabilities decrease for increasing values of the threshold and increase for higher *IM* levels, as expected. The systems with added BRBs exhibit lower conditional probabilities compared to the ones without BRBs, for the same *IM* and threshold levels, for all the monitored EDPs. Quite interestingly, also the probability of exceedance of the absolute accelerations slightly reduces due to the addition of the BRBs, whereas the infills have a minor effect on this probability.

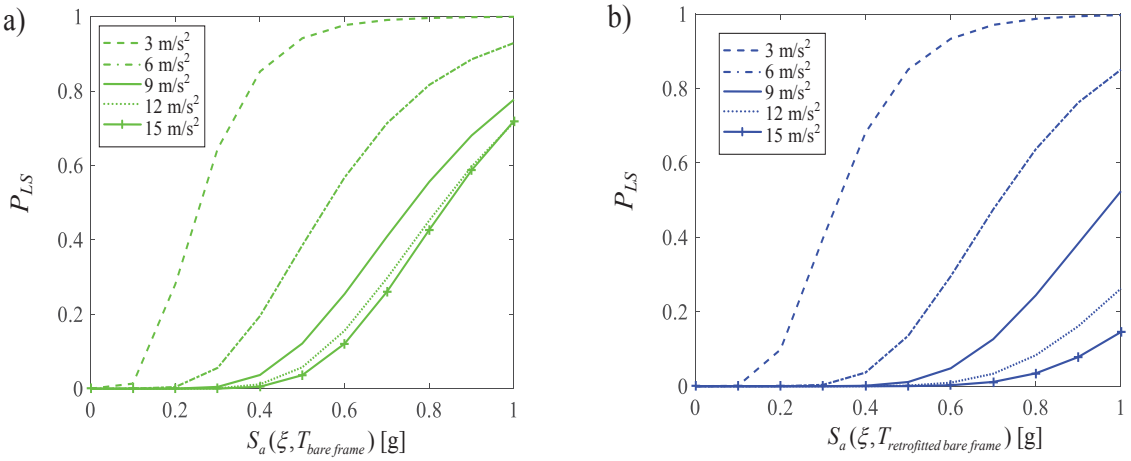

Figure 11. Conditional probability of exceedance vs. IM for the ACCs: a) Bare frame; b) Bare frame with BRBs.

It is noteworthy that the curves plotted in Figure 10-Figure 11 have been derived by considering different *IMs* for each of the models analysed. Thus, they could not be directly compared to each other. While in Freddi et al. [7] the concept of safety margin is used to compare fragility curves developed for a RC frame before and after the retrofit with BRBs, in this study seismic demand hazard curves, that are not conditional to the *IM*, are employed.

5 SEISMIC DEMAND HAZARD CURVES

Figure 12 shows the seismic hazard curves, expressing the mean annual rate (MAF) of exceedance λ of the various *IMs* considered in this study. These curves, plotted in semi-logarithmic scale, have been derived for the site in L'Aquila, where the structure is located, by following the procedure described in [34]. It can be observed that for the same level of the MAF of exceedance, the spectral acceleration is higher for the retrofitted frame than for the unretrofitted frame.

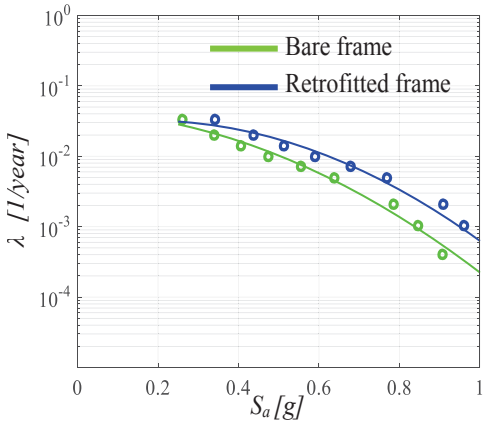

Figure 12. Seismic hazard curves for the unretrofitted frame and the frame retrofitted with BRBs obtained by neglecting the infill wall contribution.

The seismic demand hazard curves for the various systems and EDPs of interest are obtained by convolution of the conditional probability of exceedance (Figure 10 to Figure 11) with the relevant seismic hazard curve (Figure 12). The demand hazard curve for the generic EDP can be estimated as follows:

$$\lambda_{EDP}(edp) = \int_0^{\infty} G_{EDP|IM}(edp|im) \left| \frac{d\lambda_{IM}(im)}{d(im)} \right| d(im) \tag{4}$$

where $d(\cdot)$ denotes the differential operator.

Figure 13 shows the demand hazard curves of the various EDPs of interest obtained for the structural models considered.

With regard to the *IDR*, it can be observed that the BRBs are effective to reduce the seismic demand to more acceptable values. In particular, the MAF of exceedance of the 0.5% threshold, commonly associated to onset of nonlinear behaviour of the frame, reduces from 0.0164 1/year to 0.0249 1/year, whereas the MAF of exceedance of the 2% threshold, associated to significant damage to the frame, reduces from 0.0037 1/year to 0.0001 1/year. Thus, the performance improvement is higher for high drift levels. It is also interesting to observe that the MAF of exceedance of the 1.5% limit, which is considered for the design of the BRBs, is equal to $6 \cdot 10^{-4}$ 1/year for the case of the retrofitted frame. This value is lower than the MAF

of exceedance of the design seismic input, which is $2.1 \cdot 10^{-3}$ 1/year. The discrepancy may be due to the simplifying assumptions of the design procedure, particularly the fact that the isotropic hardening behavior of the BRBs is neglected when evaluating the pushover curve of the retrofitted frame. Nevertheless, the MAF of exceedance is higher than the reference MAF of collapse that is targeted by the risk-based design approaches in the US [55]. In Europe, lower values of the MAF of collapse are sought for new structures, (about 10^{-5}-10^{-6} 1/year [51], [55].

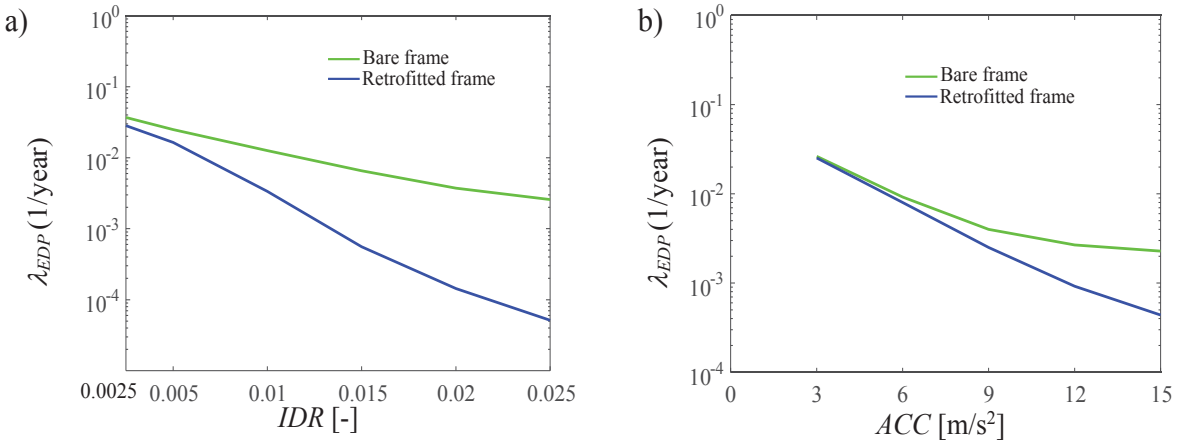

Figure 13. Demand hazard curves of the EDPs for the different structural models considered.

In Figure 13b, it is interesting to observe that the curve of the MAF of exceedance of the absolute accelerations is very similar for all the models for low acceleration values, below 9 m/s^2. This is because adding the BRBs and the infills to the frame results both in a decrease of period, which would increase the acceleration demand, but also in an increase of energy dissipation, which on the other hand reduces the acceleration demand. Thus, this type of retrofit is not very effective in improving the performance of acceleration-sensitive non-structural components. Some improvements in terms of acceleration demand reduction can be observed for acceleration value higher than 9 m/s^2. More details may be found in [56].

6 CONCLUSIONS

In this work, a performance-based approach is employed to evaluate the efficiency of the retrofitting of an existing RC building with buckling restrained braces (BRBs). In particular, an existing reinforced concrete building located in L'Aquila is used as case study. An advanced non-linear three-dimensional model of the existing RC building is defined in OpenSees, and a widely employed procedure based on pushover analyses is used to design the braces. Specifically, the bracing system is designed to obtain a retrofitted bare structure that is able to withstand the seismic demand associated to the life safety limit state design spectrum (return period of 475 years) experiencing a maximum absolute interstorey drift index of 1.5%. Successively, the seismic performance of the retrofitted bare building is evaluated by performing both non-linear static analyses and incremental dynamic analyses under a set of real ground motion records scaled to increasing seismic intensity levels. Seismic demand hazard curves are estimated for the interstorey drifts and other engineering demand parameters. The spectral acceleration at the fundamental period of the bare or infilled structure for a damping factor of 5% is used as intensity measure.

Based on the study results, the following conclusions can be drawn:

- Adding a relatively light BRB brace system to the existing frame results in notable performance improvements. In fact the use of the BRBs provides not only an increased ductility

capacity to the system, but also a reduction of the softening behavior following the attainment of the peak resistance, as shown by the capacity curves of the analysed models. The benefit in terms drift reduction due to the use of BRBs are also evident by observing the demand hazard curves for the IDRs. The MAF of exceedance of the 1.5% limit, which is considered for the design of the BRBs, is equal to $6 \cdot 10^{-4}$ 1/year for the case of the retrofitted frame with no infills, and it is about 1/10 of the corresponding MAF level for the case of the bare frame with no BRBs.

- The retrofit with BRBs does not reduce significantly the risk of exceeding absolute acceleration demands less than 9 m/s^2, but it more effective for higher acceleration levels. Thus, alternative retrofit measures may have to be employed if the seismic performance of acceleration-sensitive non-structural components has to be minimized.

REFERENCES

[1] Soong T.T., Dargush G.F. Passive Energy Dissipation Systems in Structural Engineering. Wiley & Sons, 1997.

[2] De Iuliis, M., & Castaldo, P. (2012). An energy-based approach to the seismic control of one-way asymmetrical structural systems using semi-active devices. Ingegneria Sismica-International Journal of Earthquake Engineering, 29(4), 31-42.

[3] Soong T.T., Constantinou M.C. Passive and Active Structural Vibration Control in Civil Engineering. Springer-Verlag: Wien-New York, 1994.

[4] Castaldo P., De Iuliis M. Optimal integrated seismic design of structural and viscoelastic bracing-damper systems. *Earthquake Engineering and Structural Dynamics*. 2014; **43**(12): 1809-1827.

[5] Soong T.T., Spencer B.F. Jr. Supplemental energy dissipation: state of the art and state of the practice. *Engineering Structures*. 2002; **24**: 243-259.

[6] Di Sarno L., Manfredi G. Seismic retrofitting of existing RC frames with buckling restrained braces. ATC & SEI 2009 Conference on Improving the Seismic Performance of Existing Buildings and Other Structures.

[7] Freddi F., Tubaldi E., Ragni L., Dall'Asta A. Probabilistic performance assessment of low-ductility reinforced concrete frames retrofitted with dissipative braces. *Earthquake Engineering & Structural Dynamics*. 2013; **42**(7): 993-1011.

[8] Sadeghi S., Rofooei F.R. Improving the seismic performance of diagrid structures using buckling restrained braces. *Journal of Construction Steel Research*, 2020, https://doi.org/10.1016/j.jcsr.2019.105905.

[9] Brown A.P., Aiken I.D., Jafarzadeh F.J. Buckling Restrained Braces Provide the Key to the Seismic Retrofit of the Wallace F. Bennett Federal Building. Modern Steel construction, AISC, 2001.

[10] Tremblay R., Degrange G., Blouin J. Seismic rehabilitation of a four-storey building with a stiffened bracing system. Proceedings of the 8th Canadian Conference on Earthquake Engineering, Vancouver, Canada 1999.

[11] Di Sarno L, Elnashai AS. Bracing systems for seismic retrofitting of steel frames. J Construct Steel Res 2009;65(2):452–65. http://dx.doi.org/10.1016/j.jcsr.2008.02.013.

[12] De Domenico, D., Impollonia, N., and Ricciardi, G. (2019a). Seismic retrofitting of confined masonry-RC buildings: The case study of the university hall of residence in Messina, Italy. Ingegneria Sismica 36, 54–85.

[13] Bozorgnia Y., Bertero V.V. Earthquake Engineering: From Engineering Seismology to Performance-Based Engineering. ICC-CRC Press, Boca Raton, Florida, USA 2004.

[14] Watanabe A., Hitomi Y., Saeki E., Wada A., Fujimoto M. Properties of Brace Eneased in Concrete-Filled Steel Tube. Proceedings of the 9th World Conference on Earthquake Engineering, Tokyo-Kyoto, Japan, 1988.

[15] Iwata M., Kato T., Wada A. Buckling-restrained braces as hysteretic dampers. Proc. STESSA 2000 Conf., 33-38, Montreal, Canada, August 2000.

[16] Black C., Makris N., Aiken I. Component Testing, Stability Analysis and Characterization of Buckling-Restrained Unbonded Braces. Report No. PEER 2002/08, Univ. of California, Berkeley, CA, 2002.

[17] Dall'Asta A., Ragni L., Tubaldi E., Freddi F. Design methods for existing r.c. frames equipped with elasto-plastic or viscoelastic dissipative braces. Conference: XIII National Conference ANIDIS: L'Ingegneria sismica in Italia, 2009.

[18] Di Sarno L., Manfredi G. Seismic retrofitting with buckling restrained braces: Application to an existing non-ductile RC framed building. *Soil Dynamics and Earthquake Engineering*. 2010; **30**(11): 1279-1297.

[19] Sutcu F., Takeuchi T., Matsui, R. Seismic retrofit design method for RC buildings using buckling-restrained braces and steel frames. *Journal of Constructional Steel Research*. 2014; **101**: 304-313.

[20] Güneyisi EM. Seismic reliability of steel moment resisting framed buildings retrofitted with buckling restrained braces. Earthquake Engineering and Structural Dynamics. 2012; **41**(5): 853–874.

[21] Sabelli R, Mahin SA, Chang C. Seismic demands on steel braced-frame buildings with buckling-restrained braces. *Engineering Structures*. 2003; **25**: 655-666.

[22] Erochko J., Christopoulos C., Tremblay R., and Choi, H. Residual drift response of SMRFs and BRB frames in steel buildings designed according to ASCE 7-05. *Journal of Structural Engineering*. 2011; **137**(5): 589–599.

[23] Kiggins S., Uang, C. M. Reducing residual interstory drift of buckling-restrained braced frames as a dual system. *Engineering Structures*. 2006; **28**(11): 1525–1532.

[24] Uang C.M., Nakashima M., Tsai K.C. Research and application of buckling restrained braced frames. *International Journal of Steel Structures*. 2004; **4**(4):301-13.

[25] Xie Q. State of the art of buckling-restrained braces in Asia. *Journal of constructional steel research*. 2005; **61**(6): 727-48.

[26] Takeuchi T., Ida M., Yamada S., Suzuki K. Estimation of cumulative deformation capacity of buckling restrained braces. *Journal of Structural Engineering*. 2008; **134**(5): 822-31.

[27] Andrews B.M., Fahnestock L.A. Song J. Ductility capacity models for buckling restrained braces. *Journal of Constructional Steel Research*. 2009; **65**(8-9): 1712-20.

[28] Fahnestock L. A., Ricles J. M., Sause R. Experimental evaluation of a large scale buckling-restrained braced frame. *Journal of Structural Engineering*. 2007; **133**(9): 1205 1214.

[29] Merritt S., Uang C. M., Benzoni G. Subassemblage testing of Star Seismic buckling-restrained braces. Structural Systems Research Project, Rep. No. TR-2003/04, Univ. of California at San Diego, San Diego, 2003.

[30] Zona A., Dall'Asta A. Elastoplastic model for steel buckling-restrained braces. *Journal of Constructional Steel Research*. 2012; **68**(1): 118-125.

[31] Gu, Q., Zona, A., Peng, Y., & Dall'Asta, A. (2014). Effect of buckling-restrained brace model parameters on seismic structural response. *Journal of Constructional Steel Research*, 98, 100-113.

[32] McKenna F., Fenves G.L., Scott M.H. OpenSees: Open system for earthquake engineering simulation. Pacific Earthquake Engineering Research Center, University of California, Berkeley, CA, 2006.

[33] Fajfar P. A nonlinear analysis method for performance-based seismic design. *Earthquake Spectra*. 2000; **16**(3): 573-592.

[34] Ministero delle Infrastrutture e dei Trasporti (2018). Aggiornamento delle "Norme tecniche per le costruzioni" (NTC 2018). Gazzetta Ufficiale 20/02/2017, n. 42 - Suppl. Ord. n. 8.

[35] Scott MH, Fenves GL. Plastic hinge integration methods for force-based beam-column elements. *Journal of Structural Engineering*. 2006; **132**(2): 244–252.

[36] Panagiotakos T. B., Fardis M. N. Deformations of Reinforced Concrete Members at Yielding and Ultimate. ACI Structural Journal, 2001; **98**(2): 135-148.

[37] Mander J. B., Priestley M. J., Park R. Theoretical Stress-Strain Model for Confined Concrete. *Journal of Structural Engineering*. 1988; **114**(8).

[38] Tremblay R., Poncet L., Bolduc P., Neville R., DeVall R. (2004). Testing and design of buckling restrained braces for Canadian application. Proceeding of the 13th World Conference on Earthquake Engineering, Vancouver, Canada.

[39] Cornell C.A., Krawinkler H. Progress and challenges in seismic performance assessment. PEER Center News. 2000; **4**(1): 1-3.

[40] Aslani H, Miranda E. Probability-based seismic response analysis. Engineering Structures 2005; 27(8): 1151-1163.

[41] Porter KA. (2003). An overview of PEER's performance-based earthquake engineering methodology. Proceedings of the 9th International Conference on Application of Statistics and Probability in Civil Engineering (ICASP9), San Francisco, California.

[42] Iervolino I., Cornell C.A. Record Selection for Nonlinear Seismic Analysis of Structures. *Earthquake Spectra*. 2005; **21**(3): 685–713.

[43] Shome N, Cornell C.A., Bazzurro P., Carballo J.E. Earthquake, records, and nonlinear responses. *Earthquake Spectra*. 1998; **14**(3): 469-500.

[44] Luco N., Cornell C.A. Structure-specific scalar intensity measures for near-source and ordinary earthquake ground motions. *Earthquake Spectra*. 2007; **23**(2): 357-92.

[45] Pinto P.E., Giannini R., Franchin P. Seismic Reliability Analysis of Structures, IUSS Press, Pavia, Italy, 2003.

[46] Vamvatsikos D., Cornell CA. Incremental dynamic analysis. *Earthquake Engineering and Structural Dynamics*. 2002; **31**(3): 491–514.

[47] PEER, Pacific Earthquake Engineering Research Center http://peer.berkeley.edu/

[48] ITACA, Italian Accelerometric Archive http://itaca.mi.ingv.it/ItacaNet/itaca10_links.htm

[49] ISESD, Internet-Site for European Strong-Motion Data http://www.isesd.hi.is/ESD_Local/frameset.htm

[50] Bazzurro P., Cornell C.A., Shome N, Carballo J.E. Three proposals for characterizing MDOF nonlinear seismic response. *Journal of Structural Engineering*. 1998, **124**(11), 1281-1289.

[51] Castaldo P., Palazzo B., Della Vecchia P. Life-cycle cost and seismic reliability analysis of 3D systems equipped with FPS for different isolation degrees. *Engineering Structures*. 2016; **125**: 349–363.

[52] Palazzo, B., Castaldo, P., & Della Vecchia, P. (2014, September). Seismic reliability analysis of base-isolated structures with friction pendulum system. In 2014 IEEE Workshop on Environmental, Energy, and Structural Monitoring Systems Proceedings (pp. 1-6). IEEE.

[53] Castaldo P., Alfano G. Seismic reliability-based design of hardening and softening structures isolated by double concave sliding devices, *Soil Dynamics and Earthquake Engineering*, 2020, **129**,105930.

[54] Bertero RD, Bertero VV. Performance-based seismic engineering: the need for a reliable conceptual comprehensive approach. *Earthquake Engineering and Structural Dynamics*. 2002; **31**: 627–652.

[55] Gkimprixis A., Tubaldi E., Douglas, J. Comparison of methods to develop risk-targeted seismic design maps. *Bulletin of Earthquake Engineering*. 2019; 1-26.

[56] Castaldo P., Tubaldi E., Selvi F., Gioiella L. Seismic performance of an existing RC structure retrofitted with buckling restrained braces. *Journal of Building Engineering*, 2021, 33, 101688.